# A Dual-Porosity Model for Waterflooding in Naturally Fractured Reservoirs

*Jim Douglas, Jr.*
*Jeffrey L. Hensley*
Purdue University, West Lafayette, Indiana 47907
and
*Todd Arbogast*
Rice University, Houston, Texas 77251

*Technical Report #127 / July 1990*

Appeared in Comp. Meth. in Appl. Mech. and Engng., vol. 87, 1991, pp. 157-174.

**Abstract.** A dual-porosity model for saturated, two-phase, incompressible, immiscible flow in a naturally fractured petroleum reservoir is formulated and then approximated by a finite difference procedure. Calculations are presented to indicate the behavior of the model as a function of several parameters, including the size and shape of the matrix blocks, the form of the relative permeability curves in the blocks, the inclination of the reservoir, the absolute permeabilities, and the fluid viscosities.

## 1. Introduction

A naturally fractured reservoir can be simulated as an interconnected system of fracture planes dividing the porous rock, which will be called the *matrix*, into a collection of blocks. The fractures, though very thin, have a profound effect on the flow of fluids within the reservoir. Most of the fluid resides in the matrix, where it moves very slowly. Fluid reaching the surface of a matrix block and entering the fractures flows comparatively quickly, since the fractures form paths of high permeability. Thus, a naturally fractured reservoir has an additional scale over the two occurring in a standard, unfractured reservoir. The smallest scale, on the order of millimeters, is that of the pores. The intermediate and new scale is that of the fracture spacing, which is on the order of meters. Finally, the reservoir length is on the order of kilometers.

In any practical spatial discretization of the reservoir, there will be many matrix blocks in every grid cell and we cannot and need not compute the flow of fluids within each of the individual fractures and blocks. We shall consider a dual-porosity formulation to enable us to simulate the flow in a fashion that is both computationally tractable and sufficiently precise for practical purposes. A fractured reservoir could be modeled by allowing the porosity and permeability to vary rapidly and discontinuously over the reservoir; see [5], [6], [7], [14], and [16] for a general description of flow in porous media. Both of these quantities are dramatically greater in the fractures than in the porous rock. Since the computational and data requirements for such a model would be totally impractical, this model must be rejected for practical simulation. As an alternative, one might try to avoid the discontinuous nature of the porosity and permeability by replacing them locally by their average values. While such a simulation could be done as in the unfractured case, the result would be unsatisfactory, in that correlation to physical observations would not be obtained. The interchange of fluid between the matrix and the fractures must be modeled [15], [4], [20] by treating them as if the reservoir possesses *two* porous structures rather than one. Since the system of fractures is on a much finer scale than the reservoir as a whole, it can be viewed as a porous structure itself (see Fig. 1). The fractures form the "void spaces" while the matrix blocks play the role of the "solid rock"; note that the "solid part" is in itself permeable.

It is well known how to model the flow of fluids in a single porous structure; a dual-porosity model is much more complicated. Derivations of models to simulate several varieties of flows in fractured reservoirs can be found in recent papers of Arbogast, Douglas, and Hornung. In this paper, we shall be concerned with two-phase, immiscible, incompressible flow; this is the type of flow related to the secondary recovery process known for some decades as waterflooding. See [1], [2], and [8] for models derived on the basis of either physical intuition or on homogenization, with the latter derivation beginning from the rapidly varying porosity and permeability description of fractured reservoirs mentioned above. The resulting model is presented on a double covering of the reservoir, with one cover, which we call $\Omega$, containing the fracture flow. The homogenization derivation of

the model attaches a matrix block to each point in $\Omega$, with these blocks being topologically disconnected, so that flow between a matrix block and its representative point in the fracture cover is permitted, while flow between individual blocks is not. We shall denote the matrix block over the point $x \in \Omega$ by $\Omega_x$ and set $\cup \Omega_x = \Omega_m$, which is the second cover of the reservoir. The matrix-fracture interaction on the scale of the fracture spacing must be carefully modeled. Its effect on the fracture system will be averaged over the size of an individual matrix block, which is comparable to the fracture spacing; however, the interaction must be treated on a smaller scale as far as the matrix blocks are concerned.

## 2. The Model

We consider saturated, two-phase, incompressible, immiscible flow, the phases being $o$ (oil or nonwetting phase) and $w$ (water or wetting phase), with densities and viscosities $\rho_\alpha$ and $\mu_\alpha$, $\alpha = o, w$, respectively. Let us recall the equations that govern such flow in a single porosity system. Let $s(x,t)$ denote the $w$-saturation, so that the $o$-phase has saturation $1-s$. Let $p_\alpha(x,t)$, $\alpha = o, w$, represent the pressure in the $\alpha$-phase, and denote the capillary pressure between the two phases by

$$p_c(s) = p_o - p_w; \tag{2.1}$$

$p_c(s)$ is assumed to be a function of $s$ only and typically is a decreasing function of $s$, as shown in Fig. 7. It becomes infinite as the saturation tends to the residual water saturation $s_{\min}$, and it is zero at the residual oil saturation corresponding to $s = s_{\max}$.

Relative permeability functions, $k_{r\alpha}(s)$, $\alpha = o, w$, quantify the interference to flow in each phase caused by the presence of the other. Usually, $k_{rw}(s_{\min}) = k_{ro}(s_{\max}) = 0$. If $\mathbf{k}(x)$ is the absolute permeability, then $\mathbf{k}k_{r\alpha}$ is the permeability of the rock to the $\alpha$-phase at the point $x$ with saturation $s$.

Potentials are more convenient to work with than pressures; denote them by

$$\psi_\alpha = p_\alpha - \rho_\alpha g z, \quad \alpha = o, w, \tag{2.2}$$

where $g$ is the gravitational constant (not vector) and $z(x)$ is the depth. Darcy's law for the volumetric flow rates in two-phase flow takes the form

$$v_\alpha = -\lambda_\alpha(s)\, \nabla \psi_\alpha, \quad \alpha = o, w, \tag{2.3}$$

where the phase mobilities are defined by

$$\lambda_\alpha(s) = \frac{\mathbf{k}k_{r\alpha}(s)}{\mu_\alpha}, \quad \alpha = o, w. \tag{2.4}$$

Incompressibility and conservation of mass (or, equivalently, volume) imply that

$$\phi \frac{\partial s}{\partial t} + \nabla \cdot v_w = q_{\text{ext},w}, \tag{2.5}$$

$$-\phi \frac{\partial s}{\partial t} + \nabla \cdot v_o = q_{\text{ext},o}, \tag{2.6}$$

where $q_{\text{ext},\alpha}$ is the external volumetric $\alpha$-source.

Define a "capillary potential" by

$$\psi_c = \psi_o - \psi_w = p_c(s) - (\rho_o - \rho_w)gz, \tag{2.7}$$

and use it and $\psi_w$ as the primary dependent variables. Then,

$$s = p_c^{-1}(\psi_c + (\rho_o - \rho_w)gz) \tag{2.8}$$

is defined from $\psi_c$ and

$$v_o = -\lambda_o(s)\nabla(\psi_w + \psi_c). \tag{2.9}$$

Finally, define a total volumetric flow rate and a total mobility by

$$v = v_o + v_w = -\lambda(s)\,\nabla\psi_w - \lambda_o(s)\nabla\psi_c, \tag{2.10}$$

$$\lambda(s) = \lambda_w(s) + \lambda_o(s), \tag{2.11}$$

respectively, and add (2.5) and (2.6) to obtain a *pressure* equation,

$$\nabla \cdot v = q_{\text{ext}}, \tag{2.12}$$

where $q_{\text{ext}} = q_{\text{ext},o} + q_{\text{ext},w}$ is the total external volumetric source. Then, (2.5) is called the *saturation* equation.

In summary, the basic equations for describing two-phase, incompressible, immiscible flow in a single porosity system are given by (2.3), (2.5), (2.8), and either (2.6) and (2.9) or (2.10)-(2.12).

There exists an extensive literature on the modeling of immiscible flow in naturally fractured reservoirs, including [11], [12], [13], [17], [18], and [19]. Most of these papers consider models that effectively define the matrix-fracture interaction by introducing various *ad hoc* parameters; the others do not incorporate the matrix boundary condition in any general way. We consider here a model that treats the interaction explicitly through boundary conditions on the matrix blocks [1], [2], [8], [3].

We denote fracture quantities by upper case letters and matrix quantities by corresponding lower case letters.

Capillary pressure and relative permeability functions are somewhat different in the fractures than in the matrix blocks. Generally, one assumes that the fractures are essentially like spaces between two parallel planes and that $S_{\min} = 0$ and $S_{\max} = 1$. Typical examples are shown in Fig. 9.

There are matrix source terms $q_{m,\alpha}$, $\alpha = o, w$, for each of the phases. The saturation, pressure, and capillary equations in the fracture system can be written as

$$\Phi \frac{\partial S}{\partial t} - \nabla \cdot [\Lambda_w(S)\nabla\Psi_w] = q_{\text{ext},w} + q_{m,w} \quad \text{for } x \in \Omega,\ t > 0, \tag{2.13}$$

$$-\nabla \cdot [\Lambda(S)\nabla\Psi_w + \Lambda_o(S)\nabla\Psi_c] = q_{\text{ext}} \quad \text{for } x \in \Omega,\ t > 0, \tag{2.14}$$

$$S = P_c^{-1}\big(\Psi_c + (\rho_o - \rho_w)gz\big), \tag{2.15}$$

since incompressibility requires that $q_{m,o} + q_{m,w} = 0$. The equations on the block $\Omega_x$ are

$$\phi \frac{\partial s}{\partial t} - \nabla \cdot [\lambda_w(s)\nabla\psi_w] = 0 \quad \text{for } y \in \Omega_x,\ t > 0, \tag{2.16}$$

$$-\nabla \cdot [\lambda(s)\nabla\psi_w + \lambda_o(s)\nabla\psi_c] = 0 \quad \text{for } y \in \Omega_x,\ t > 0, \tag{2.17}$$

$$s = p_c^{-1}\big(\psi_c + (\rho_o - \rho_w)gz\big); \tag{2.18}$$

we have assumed that the external sources affect the fracture system only. The boundary conditions for the matrix problems are given by requiring continuity of the potentials:

$$\psi_w(x, y, t) = \Psi_w(x, t) \quad \text{for } y \in \partial\Omega_x,\ x \in \Omega,\ t > 0, \tag{2.19}$$

and

$$\psi_c(x, y, t) = \Psi_c(x, t) \quad \text{for } y \in \partial\Omega_x,\ x \in \Omega,\ t > 0. \tag{2.20}$$

The matrix source terms are defined as follows. The volume of the $w$-fluid leaving the block $\Omega_x$ is

$$\int_{\partial\Omega_x} v_w \cdot n\, da(y) = \int_{\Omega_x} \nabla \cdot v_w\, dy = -\int_{\Omega_x} \phi \frac{\partial s}{\partial t}\, dy; \tag{2.21}$$

consequently, let

$$q_{m,w}(x, t) = -\frac{1}{|\Omega_x|} \int_{\Omega_x} \phi \frac{\partial s}{\partial t}\, dy \quad \text{for } x \in \Omega,\ t > 0. \tag{2.22}$$

We complete the model by specifying the external boundary conditions and the initial conditions for the system. For the case of no flow across the external boundary,

$$\Lambda_\alpha(s)\, \nabla \Psi_\alpha \cdot n = 0 \quad \text{for } x \in \partial\Omega,\ t > 0,\ \alpha = o, w, c. \tag{2.23}$$

Initial saturations (i.e., capillary potentials) must be specified:

$$\Psi_c(x, 0) = \Psi_{\text{init},c}(x) \quad \text{for } x \in \Omega, \tag{2.24}$$

$$\psi_c(x, 0) = \psi_{\text{init},c}(x) \quad \text{for } x \in \Omega_m. \tag{2.25}$$

To be consistent, (2.19), (2.20), and (2.23) should hold when $t = 0$.

## 3. A Finite Difference Discretization Technique

A finite difference procedure for approximating the solution to the model will be introduced, with an emphasis being placed on solving the matrix equations essentially independently of the fracture equations. It is important practically to solve the matrix equations in a manner that allows an implicit treatment of the overall system, while confining the nonlinearities of the algebraic problem at each time step to the fracture system. The fracture and matrix systems cannot be handled sequentially, since a small change in the boundary values on each matrix block can cause flow of a volume of fluid that is large in comparison to the volume of the fractures, causing numerical oscillations to occur as a result of the matrix absorbing more fluid from the surrounding fractures on one step than can be resident there and then returning more to the fractures on the next step than their total volume. The matrix-fracture interaction must be handled *implicitly*; we shall compute this interaction by a particular linearization of the matrix problems to be made precise below. The final procedure requires solution of a large nonlinear system, corresponding to the fracture equations, and many small linear systems, each corresponding to a matrix block approximated by a modest number of nodes. The fracture system typically involves about as many nodes as are used in simulation of an unfractured reservoir. However the algebraic equations generated on each time step are solved, the separation procedure detailed below will lead to more efficient computation, but there is an added advantage of the separation when it is carried out on a parallel computer, since matrix blocks interact only through the fracture system and do not directly affect each other. As a consequence, it is natural to solve the matrix problems in parallel, and little communication of data between processors is required. The algebraic equations in the fractures can be treated either by domain decomposition techniques to solve the fracture equations in parallel or on a vector processor.

Let us introduce some notation. Discretize the time variable by choosing $t^0, t^1, t^2, \ldots, t^N$ such that $0 = t^0 < t^1 < t^2 < \cdots < t^N$ and set $\Delta t^n = t^n - t^{n-1}$. Discretize the space variables by defining grids over $\Omega$ and over each matrix block $\Omega_x$. In a finite difference context, it is simplest to consider $\Omega$ and $\Omega_x, x \in \Omega$, to be rectangular parallelepipeds; more general domains can be treated by either finite difference or finite element techniques quite analogous to the finite difference methods to be described herein. Suppose that $\Omega = [0, D_1] \times [0, D_2] \times [0, D_3]$. Then, divide each $D_j$ into $N_j$ intervals, which for simplicity we take to be of equal size $H_j = D_j/N_j$, $j = 1, 2, 3$. Thus, the fracture grid is the lattice of points

$$\mathcal{G}_f = \{x_L : L = (L_1, L_2, L_3),\ x_L = (L_1 H_1, L_2 H_2, L_3 H_3),$$
$$\text{and } L_j = 0, 1, 2, \ldots, N_j,\ j = 1, 2, 3\}.$$

Again for notational convenience assume that the matrix blocks are all of the same

size and consider a grid defined on the representative matrix block $\mathcal{Q}_m$. Let $h_j$ and $n_j$ be analogous to $H_j$ and $N_j$ and set

$$\mathcal{G}_m = \{y_\ell : \ell = (\ell_1, \ell_2, \ell_3),\ y_\ell = (\ell_1 h_1, \ell_2 h_2, \ell_3 h_3),\ \text{and}\ \ell_j = 0, 1, 2, \ldots, n_j,\ j = 1, 2, 3\}.$$

Also, let

$$\overset{\circ}{\mathcal{G}}_m = \{y_\ell : \ell = (\ell_1, \ell_2, \ell_3),\ y_\ell = (\ell_1 h_1, \ell_2 h_2, \ell_3 h_3),\ \text{and}\ \ell_j = 1, 2, \ldots, n_j - 1,\ j = 1, 2, 3\}$$

indicate the interior nodes and $\partial\mathcal{G}_m = \mathcal{G}_m \setminus \overset{\circ}{\mathcal{G}}_m$ the boundary nodes. (In practice the matrix grid should be graded to place more nodes near the surface of the block. Advantage should be taken of the symmetry of the solution on a matrix block to allow the solution to be computed only at necessary nodes.)

We wish to approximate solutions at time levels $t^n$. An approximation to a function $\Theta$ related to the the fracture system at a point $x_L \in \mathcal{G}_f$ will be denoted by

$$\Theta_L^n \approx \Theta(x_L, t^n).$$

Each $H_j$ will normally be considerably larger than the spacing of the fracture planes. Only those blocks which sit over the points of $\mathcal{G}_f$ will enter the discretization process. For a function $\theta$ associated with the block at the point $x_L \in \mathcal{G}_f$ denote the approximation to $\theta$ at $y_\ell \in \mathcal{G}_m$ by

$$\theta_{L,\ell}^n \approx \theta(x_{L,\ell}, t^n),$$

where $x_{L,\ell} = x_L - y_\ell$ (we assume that a top corner of the block is $x_L$).

Time derivatives will be discretized by backward Euler approximations. Grid points spatially adjacent to a given point $x_L$ are denoted by $x_{L\pm e_j}$, where $e_1 = (1,0,0)$, $e_2 = (0,1,0)$, and $e_3 = (0,0,1)$. Points half-way between $x_L$ and $x_{L\pm e_j}$ are denoted by $x_{L\pm\frac{1}{2}e_j}$. A similar notation will be employed for points adjacent to $x_{L,\ell}$.

The matrix equations will be completely linearized, but *not* the fracture equations. A Newton-like iteration will be used to solve the nonlinear equations of the discretized fracture system; the discrete matrix system is directly solvable. The five parts of the algorithm below uncouple the calculations related to the matrix blocks from those of the fracture calculation:

i) **Initialization.** For each $L$ and $l$,

$$\Psi_{c,L}^0 = \Psi_{\text{init},c}(x_L), \tag{3.1}$$

$$\psi_{c,L,\ell}^0 = \psi_{\text{init},c,L,\ell}(x_{L,\ell}), \tag{3.2}$$

$$S_L^0 = P_c^{-1}\left(\Psi_{c,L}^0 + (\rho_o - \rho_w) g\, z(x_L)\right), \tag{3.3}$$

$$s_{L,\ell}^0 = p_c^{-1}\left(\psi_{c,L,\ell}^0 + (\rho_o - \rho_w) g\, z(x_{L,\ell})\right). \tag{3.4}$$

The initial water potentials can be determined by solving (3.22) and (3.30) below. The Newton procedure will require an initial guess at the solution, so that $\Psi^0_{w,L}$ should be found; the initial matrix water potential is not needed.

ii) **Matrix system.** For each $L$, $\ell$, and for $n \geq 1$, find $\{\bar{\psi}^n_{c,L,\ell}, \bar{\psi}^n_{w,L,\ell}\}$ by solving

$$\phi(x_{L,\ell}) \frac{\bar{\psi}^n_{c,L,\ell} - \psi^{n-1}_{c,L,\ell}}{p'_c(s^{n-1})\Delta t^n} - \nabla_{h,L,\ell} \cdot \left[\lambda_w(s^{n-1}) \nabla_{h,L,\ell} \bar{\psi}^n_w\right] = 0 \quad \text{if } y_\ell \in \mathring{\mathcal{G}}_m, \tag{3.5}$$

$$- \nabla_{h,L,\ell} \cdot \left[\lambda(s^{n-1}) \nabla_{h,L,\ell} \bar{\psi}^n_w + \lambda_o(s^{n-1}) \nabla_{h,L,\ell} \bar{\psi}^n_c\right] = 0 \quad \text{if } y_\ell \in \mathring{\mathcal{G}}_m, \tag{3.6}$$

$$\bar{\psi}^n_{c,L,\ell} = \Psi^{n-1}_{c,L} \quad \text{if } y_\ell \in \partial\mathcal{G}_m, \tag{3.7}$$

$$\bar{\psi}^n_{w,L,\ell} = \Psi^{n-1}_{w,L} \quad \text{if } y_\ell \in \partial\mathcal{G}_m, \tag{3.8}$$

and determine $\{\breve{\psi}^n_{c,L,\ell}, \breve{\psi}^n_{w,L,\ell}\}$ and $\{\hat{\psi}^n_{c,L,\ell}, \hat{\psi}^n_{w,L,\ell}\}$ by solving

$$\phi(x_{L,\ell}) \frac{\breve{\psi}^n_{c,L,\ell}}{p'_c(s^{n-1})\Delta t^n} - \nabla_{h,L,\ell} \cdot \left[\lambda_w(s^{n-1}) \nabla_{h,L,\ell} \breve{\psi}^n_w\right] = 0 \quad \text{if } y_\ell \in \mathring{\mathcal{G}}_m, \tag{3.9}$$

$$- \nabla_{h,L,\ell} \cdot \left[\lambda(s^{n-1}) \nabla_{h,L,\ell} \breve{\psi}^n_w + \lambda_o(s^{n-1}) \nabla_{h,L,\ell} \breve{\psi}^n_c\right] = 0 \quad \text{if } y_\ell \in \mathring{\mathcal{G}}_m, \tag{3.10}$$

$$\breve{\psi}^n_{c,L,\ell} = 1 \quad \text{if } y_\ell \in \partial\mathcal{G}_m, \tag{3.11}$$

$$\breve{\psi}^n_{w,L,\ell} = 0 \quad \text{if } y_\ell \in \partial\mathcal{G}_m, \tag{3.12}$$

and

$$\phi(x_{L,\ell}) \frac{\hat{\psi}^n_{c,L,\ell}}{p'_c(s^{n-1})\Delta t^n} - \nabla_{h,L,\ell} \cdot \left[\lambda_w(s^{n-1}) \nabla_{h,L,\ell} \hat{\psi}^n_w\right] = 0 \quad \text{if } y_\ell \in \mathring{\mathcal{G}}_m, \tag{3.13}$$

$$- \nabla_{h,L,\ell} \cdot \left[\lambda(s^{n-1}) \nabla_{h,L,\ell} \hat{\psi}^n_w + \lambda_o(s^{n-1}) \nabla_{h,L,\ell} \hat{\psi}^n_c\right] = 0 \quad \text{if } y_\ell \in \mathring{\mathcal{G}}_m, \tag{3.14}$$

$$\hat{\psi}^n_{c,L,\ell} = 0 \quad \text{if } y_\ell \in \partial\mathcal{G}_m, \tag{3.15}$$

$$\hat{\psi}^n_{w,L,\ell} = 1 \quad \text{if } y_\ell \in \partial\mathcal{G}_m, \tag{3.16}$$

where

$$\nabla_{h,L,\ell} \cdot \left[\lambda_\alpha(s^{n-1}) \nabla_{h,L,\ell} \psi^n\right] = \sum_{j=1}^{3} \frac{1}{h_j^2} \left\{ \lambda_\alpha\left(\frac{s^{n-1}_{L,\ell+e_j} + s^{n-1}_{L,\ell}}{2}\right)(\psi^n_{L,\ell+e_j} - \psi^n_{L,\ell}) \right.$$
$$\left. - \lambda_\alpha\left(\frac{s^{n-1}_{L,\ell} + s^{n-1}_{L,\ell-e_j}}{2}\right)(\psi^n_{L,\ell} - \psi^n_{L,\ell-e_j}) \right\}. \tag{3.17}$$

Note that these equations are indeed linear, since the mobilities and $p_c'$ are evaluated at the previous time level. The matrix potentials $\psi^n_{c,L,\ell}$ and $\psi^n_{w,L,\ell}$ are defined below in (3.26) and (3.27); they satisfy the expected equations, namely (3.29)-(3.32). Equations (3.5)-(3.8) define a particular solution to the linear equations, while (3.9)-(3.12) and (3.13)-(3.16) give solutions to the homogeneous problems which describe unit changes in the boundary conditions.

iii) **The matrix source term.** For each $L$ and $n \geq 1$,

$$\tilde{\psi}^n_{w,L,\ell} = \bar{\psi}^n_{w,L,\ell} + \left(\Psi^n_{c,L} - \Psi^{n-1}_{c,L}\right) \check{\psi}^n_{w,L,\ell} + \left(\Psi^n_{w,L} - \Psi^{n-1}_{w,L}\right) \hat{\psi}^n_{w,L,\ell}, \tag{3.18}$$

$$\tilde{s}^n_{L,\ell} = p_c^{-1}\left(\tilde{\psi}^n_{w,L,\ell} + (\rho_o - \rho_w) g z(x_{L,\ell})\right), \tag{3.19}$$

$$q^n_{m,w,L} = -\frac{1}{|\mathcal{Q}_m|} \sum_{\ell} \phi(x_{L,\ell}) \frac{\tilde{s}^n_{L,\ell} - s^{n-1}_{L,\ell}}{\Delta t^n} h_1 h_2 h_3. \tag{3.20}$$

The quantity $q^n_{m,w,L}$ is given implicitly in terms of the fracture potentials at the $n$th time level; however, in view of (3.27) and (3.28) below, (3.20) is clearly a discretization of (2.22).

iv) **Fracture system.** (This is the most critical system to solve well.) For each $L$ and $n \geq 1$, solve the following nonlinear system of equations for $\Psi^n_{c,L}$, $\Psi^n_{w,L}$, $S^n_L$ and $q^n_{m,w,L}$:

$$\begin{aligned} \Phi(x_L) \frac{S^n_L - S^{n-1}_L}{\Delta t^n} - \sum_{j=1}^{3} \frac{1}{H_j^2} \Big\{ & \Lambda^n_{w,L,j}\left(\Psi^n_{w,L+e_j} - \Psi^n_{w,L}\right) \\ & - \Lambda^n_{w,L-e_j,j}\left(\Psi^n_{w,L} - \Psi^n_{w,L-e_j}\right)\Big\} \\ = q_{\mathrm{ext},w}(x_L, t^n) + q^n_{m,w,L}, & \end{aligned} \tag{3.21}$$

$$\begin{aligned} - \sum_{j=1}^{3} \frac{1}{H_j^2} \Big\{ & \Lambda^n_{L,j}\left(\Psi^n_{w,L+e_j} - \Psi^n_{w,L}\right) - \Lambda^n_{L-e_j,j}\left(\Psi^n_{w,L} - \Psi^n_{w,L-e_j}\right) \\ & + \Lambda^n_{o,L,j}\left(\Psi^n_{c,L+e_j} - \Psi^n_{c,L}\right) - \Lambda^n_{o,L-e_j,j}\left(\Psi^n_{c,L} - \Psi^n_{c,L-e_j}\right)\Big\} \\ = q_{\mathrm{ext}}(x_L, t^n), & \end{aligned} \tag{3.22}$$

$$S^n_L = P_c^{-1}\left(\Psi^n_{c,L} + (\rho_o - \rho_w) g z(x_L)\right), \tag{3.23}$$

where the no-flow boundary conditions of (2.23) are imposed by reflection:

$$\Psi^n_{\alpha,L\pm e_j} = \Psi^n_{\alpha,L\mp e_j}, \quad \alpha = w, c, \tag{3.24}$$

if $x_{L\pm e_j}$ is outside the reservoir. The mobilities should be upstream weighted:

$$\Lambda^n_{\alpha,L,j} = \begin{cases} \Lambda_\alpha(S^n_{L+e_j}), & \text{if } \Psi^n_{\alpha,L} < \Psi^n_{\alpha,L+e_j}, \\ \Lambda_\alpha(S^n_L), & \text{otherwise,} \end{cases} \tag{3.25}$$

for $\alpha = o, w$ (where $\Psi^n_{o,L} = \Psi^n_{c,L} + \Psi^n_{w,L}$). This is intended to prevent numerical instabilities; see [9], [14].

Note that (3.18)-(3.25) form a completely implicit procedure for the fracture quantities and the boundary values on the blocks. Indeed, the equations can be interpreted as a system of nonlinear equations in the fracture quantities alone, and a variant of Newton's method can be used to obtain the solution; this is not completely straightforward, because of sharp corners at $S_{\max}$ or $s_{\max}$ in the graphs of the capillary functions (Figs. 7 and 9). Since the rate of convergence in a Newton iteration is related to the value of the second derivatives (which fail to exist at the corners of the capillary curves), it is necessary to modify the algorithm so as to aid the convergence by, for example, requiring the solution $\Psi_c$ to take at least two iterations to cross a value slightly above the critical value $\Psi_{c,L} = P_c(S_{\max}) - (\rho_o - \rho_w)gz = -(\rho_o - \rho_w)gz$ at any applicable point. It is also necessary to require that $P_c'(S_{\max}) = p_c'(s_{\max}) = -\infty$ (or a large negative number in practice).

v) **Matrix update.** For each $L, \ell$, and $n \geq 1$, let

$$\psi^n_{c,L,\ell} = \bar{\psi}^n_{c,L,\ell} + \left(\Psi^n_{c,L,\ell} - \Psi^{n-1}_{c,L,\ell}\right)\breve{\psi}^n_{c,L,\ell} + \left(\Psi^n_{w,L,\ell} - \Psi^{n-1}_{w,L,\ell}\right)\hat{\psi}^n_{c,L,\ell}, \tag{3.26}$$

$$\psi^n_{w,L,\ell} = \bar{\psi}^n_{w,L,\ell} + \left(\Psi^n_{c,L,\ell} - \Psi^{n-1}_{c,L,\ell}\right)\breve{\psi}^n_{w,L,\ell} + \left(\Psi^n_{w,L,\ell} - \Psi^{n-1}_{w,L,\ell}\right)\hat{\psi}^n_{w,L,\ell}, \tag{3.27}$$

$$s^n_{L,\ell} = p_c^{-1}\left(\psi^n_{c,L,\ell} + (\rho_o - \rho_w)gz(x_{L,\ell})\right). \tag{3.28}$$

This completes the time step.

The above algorithm can be implemented sequentially. The following discrete matrix problem has been solved:

$$\phi(x_{L,\ell})\,\frac{\psi^n_{c,L,\ell} - \psi^{n-1}_{c,L,\ell}}{p_c'(s^{n-1})\Delta t^n} - \nabla_{h,L,\ell}\cdot\left[\lambda_w(s^{n-1})\nabla_{h,L,\ell}\,\psi^n_w\right] = 0 \quad \text{if } y_\ell \in \mathring{\mathcal{G}}_m, \tag{3.29}$$

$$-\nabla_{h,L,\ell}\cdot\left[\lambda(s^{n-1})\nabla_{h,L,\ell}\,\psi^n_w + \lambda_o(s^{n-1})\nabla_{h,L,\ell}\,\psi^n_c\right] = 0 \quad \text{if } y_\ell \in \mathring{\mathcal{G}}_m, \tag{3.30}$$

$$\psi^n_{c,L,\ell} = \Psi^n_{c,L} \quad \text{if } y_\ell \in \partial\mathcal{G}_m, \tag{3.31}$$

$$\psi^n_{w,L,\ell} = \Psi^n_{w,L} \quad \text{if } y_\ell \in \partial\mathcal{G}_m. \tag{3.32}$$

Assuming that the wetting fluid is the denser, it should be noted that the block associated with the fracture point $x_L$ is interpreted to lie below $x_L$ for imbibition and above for drainage; otherwise, fluid is trapped by the numerical simulation as $P_c$ tends to zero. We have considered the case of imbibition.

It should be remarked that the discretization of the fracture system conserves mass, except for inexactness caused by not carrying out the Newton iteration to complete convergence. The linearized matrix problems do not; however, there is no *net* mass balance

error, as any fluid that leaves the matrix is transmitted to the fracture system. There is a small error in the time at which fluid is transferred from one system to the other.

## 4. Results of Experimental Calculations

We consider some simulations of waterflooding and present the results of the experimental calculations. Recovery curves will be shown to indicate the dependence of the solution on a variety of parameters including the block size and shape, the form of the relative permeability curves in the blocks, the inclination of the reservoir, the absolute permeabilities, and the fluid viscosities. Though these curves give only a gross indication of the flow of fluids within the reservoir, they are sufficient to illustrate important features of the simulations. (A recovery curve is the graph of the cumulative amount of oil produced versus the cumulative amount of water injected.)

The reservoir is assumed rectangular, with height 10 meters and length 300 meters. For computational simplicity, the reservoir is assumed to be uniform in the other direction; consequently, the fracture calculations are two-dimensional over $\Omega$, though the matrix calculations must remain three-dimensional over each $\Omega_x$. Initially, the reservoir contains 75% oil and 25% water. Water is injected uniformly into the reservoir along one end at a constant rate of one pore-volume every five years; calculations not reported here indicated that the qualitative behavior of the system is relatively independent of the injection rate. Oil and water are produced at the top of the other end. Given the porosities assumed below, there is a maximum recovery of about .65 pore-volumes.

The following data are held fixed for most of the computational results exhibited below:

| | | |
|---|---|---|
| Fluid properties: | | |
| Viscosity | $\mu_w = .5$ cP | $\mu_o = 2$ cP |
| Density | $\rho_w = 1\ g/\,\mathrm{cm}^3$ | $\rho_o = .7\ g/\,\mathrm{cm}^3$ |
| Absolute Permeabilities | $K = 1$ darcy | $k = 0.05$ darcy |
| Porosities: | $\Phi = .01$ | $\phi = .2$ |
| Residual Saturations (matrix) | $s_{ro} = .15$ | $s_{rw} = .2$ |
| Residual Saturations (fractures) | $S_{ro} = 0$ | $S_{rw} = 0$ |

The capillary pressure functions were assumed in the form

$$
\begin{aligned}
P_c(S) &= (1-S)\{\gamma(S^{-1}-1)+\Theta\},\\
p_c(s) &= \alpha(\{s_0 - s + \beta\}^{1/2} - \beta^{1/2})(s - s_{rw})^{-2},\\
s_0 &= 1 - s_{ro}, \qquad \beta = s_{ro}^2(s_0 - s_{rw})^{-2},\\
\gamma &= 2.0 \times 10^4 \text{ dynes}/\,\mathrm{cm}^2, \quad \Theta = 100 \text{ dynes}/\,\mathrm{cm}^2,\\
\alpha &= 3.0 \times 10^3 \text{ dynes}/\,\mathrm{cm}^2 .
\end{aligned}
$$

The relative permeabilty functions in the fractures were chosen to be linear, with the residual saturations taken to be zero:

$$K_{ro}(S) = 1 - S, \qquad K_{rw}(S) = S.$$

Several forms were assumed for the relative permeability functions in the matrix blocks:

$$i) \qquad k_{ro}(s) = (1 - s_e)^{\zeta_o}, \qquad k_{rw}(s) = \left(\frac{s - s_{rw}}{1 - s_{rw}}\right)^{\zeta_w}, \quad \zeta_\alpha = 2, 3, 4,$$

$$ii) \qquad k_{ro}(s) = (1 - s_e)^2(1 - s_e^2), \quad k_{rw}(s) = \left(\frac{s - s_{rw}}{1 - s_{rw}}\right)^4, \quad s_e(s) = s/(1 - s_{ro}).$$

For the finite difference procedure described above, earlier tests [8] [9] demonstrated that the relatively coarse discretization of 40 horizontal nodes and 10 vertical nodes in the fracture domain provides accurate recovery curves. In each matrix block over a fracture grid point, we took the equivalent of 16 interior nodes (four nodes on each of four horizontal planes). The time step varied from one-fourth day to one day initially to a maximum of ten days near the end of the simulations. (An entire simulation was for about twenty years.)

The first figure indicates a significant dependence of the recovery on the form of the relative permeability functions in the matrix blocks, with an apparent greater dependence on the relative permeability to the oil phase than to that for the water phase. The most rapid recovery was obtained for the choices $\zeta_o = \zeta_w = 2$ in the forms $i)$ above. Shifting $\zeta_w$ to four, while holding $\zeta_o$ at two, had a negligible effect on recovery. Increasing both exponents to three reduced the recovery rate strongly. Recovery for relative permeabilities in the forms $ii)$ fell between these curves. These results agree with the physical intuition that recovery should be slowed by increasing resistance to flow.

Block size also affects recovery rates significantly. Figures 2, 3, and 4 indicate that, as the side length of cubic blocks tends to zero, the recovery curves converge upwards to the corresponding recovery curve given by a limit model [8] [9] [10] derived by taking a formal limit of this model (and one in which gravity is neglected in the blocks [3] [8] [9]); this behavior holds for relative permeability curves of either of the above forms. Including the effect of gravity in the blocks is important; the model of [3] and [8] ignored it. In Figure 5 it is clear that a much better recovery is predicted when the gravitational effects in the blocks are included; the recovery curves labelled "no gravity" were computed using the full model with the gravitational constant set to zero just in the blocks. When gravity is omitted in the blocks, it is possible to reduce the differential equations in a block to a single equation for the saturation; this was done in [3] and [9] and called the "small block model" [8]. Figure 6 shows that the the models are consistent; the small variance in the recovery rates are due to a difference in the spatial discretizations in the two codes.

In Figures 7 and 8 we see the importance of block geometry on production. For the relatively tall block of height 200 cm, recovery is improved as the horizontal cross-section

is reduced; clearly, a smaller cross-section allows imbibition to be more dominant in the displacement process in the blocks. For a somewhat shorter block of height 100 cm, changing the cross-section seems less important.

In Figure 9 the effect of inclining the reservoir by an angle $\theta$ is studied ($\theta > 0$ indicates that the production corner is above the injection side of the reservoir). Increasing the angle improves oil production. Figure 10 shows the effect of increasing oil viscosity; oil recovery is significantly slowed by increasing oil viscosity. Figure 11 presents the effect of changing fracture permeability. Higher fracture permeability allows water more easily to bypass the matrix blocks, resulting in earlier water production. Conversely, increasing the matrix block permeability would delay water production, thereby increasing early recovery.

**Acknowledgement.** The work of Arbogast and Douglas was supported in part by the National Science Foundation and and that of Hensley in part by the U.S. Army.

REFERENCES

[1] T. ARBOGAST, J. DOUGLAS, JR., and U. HORNUNG, *Modeling of naturally fractured reservoirs by formal homogenization techniques*, to appear.

[2] ———, *Derivation of the double porosity model of single phase flow via homogenization theory*, to appear in SIAM J. Math. Anal., 21 (1990).

[3] T. ARBOGAST, J. DOUGLAS, JR., and J. E. SANTOS, *Two-phase immiscible flow in naturally fractured reservoirs*, in Numerical Simulation in Oil Recovery, M. F. Wheeler, ed., The IMA Volumes in Mathematics and its Applications, 11, Springer-Verlag, Berlin and New York, 1988, pp. 47–66.

[4] G. I. BARENBLATT, I. P. ZHELTOV, and I. N. KOCHINA, *Basic concepts in the theory of seepage of homogeneous liquids in fissured rocks [strata]*, Prikl. Mat. Mekh., 24 (1960), pp. 852–864. J. Appl. Math. Mech., 24 (1960), pp. 1286–1303.

[5] J. BEAR, *Dynamics of Fluids in Porous Media*, Dover Publication, Inc, New York, 1988.

[6] G. CHAVENT AND J. JAFFRÉ, *Mathematical Models and Finite Elements for Reservoir Simulation*, North-Holland, Amsterdam, 1986.

[7] R. E. COLLINS, *Flow of Fluids Through Porous Materials*, Reinhold, New York, 1961.

[8] J. DOUGLAS, JR. AND T. ARBOGAST, *Dual porosity models for flow in naturally fractured reservoirs*, in Dynamics of Fluids in Hierarchical Porous Media, J. H. Cushman, ed., Academic Press, 1990.

[9] J. DOUGLAS, JR., T. ARBOGAST, and P. J. PAES LEME, *Two models for the waterflooding of naturally fractured reservoirs*, in Proceedings, Tenth SPE Symposium on Reservoir Simulation, Society of Petroleum Engineers, Dallas, Texas, 1989, pp. 219–225, Paper SPE 18425.

[10] J. DOUGLAS, JR. AND P. J. PAES LEME, *A limit form of the equations for immiscible displacement in a fractured reservoir*, to appear.

[11] J. R. GILMAN, *An efficient finite–difference method for simulating phase segregation in the matrix blocks in double–porosity reservoirs*, Soc. Petroleum Engr. J., 26 (1986), pp. 403–413.

[12] H. KAZEMI AND J. R. GILMAN, *Improvements in simulation of naturally fractured reservoirs*, Soc. Petroleum Engr. J., 23 (1983), pp. 695–707.

[13] ———, *Improved calculations for viscous and gravity displacement in matrix blocks in dual–porosity simulators*, in Proceedings, Ninth SPE Symposium on Reservoir Simulation, Society of Petroleum Engineers, Dallas, Texas, 1987, pp. 193–208, Paper SPE 16010.

[14] D. W. PEACEMAN, *Fundamentals of Numerical Reservoir Simulation*, Elsevier, New York, 1977.

[15] S. J. PIRSON, *Performance of fractured oil reservoirs*, Bull. Amer. Assoc. Petroleum Geologists, 37 (1953), pp. 232–244.

[16] A. E. SCHEIDEGGER, *The Physics of Flow Through Porous Media*, University of Toronto Press, Third Edition, Toronto, 1974.

[17] F. SONIER, P. SOUILLARD, and F. T. BLASKOVICH, *Numerical simulation of naturally fractured reservoirs*, Proceedings, 61st Annual Technical Conference and Exhibition of the Society of Petroleum Engineers, Dallas, Texas, 1986, Paper SPE 15627.

[18] A. de SWAAN, *Theory of waterflooding in fractured reservoirs*, Soc. Petroleum Engr. J., 18 (1978), pp. 117–122.

[19] L. K. THOMAS, T. N. DIXON, and R. G. PIERSON, *Fractured reservoir simulation*, Soc. Petroleum Engr. J., 23 (1983), pp. 42–54.

[20] J. E. WARREN AND P. J. ROOT, *The behavior of naturally fractured reservoirs*, Soc. Petroleum Engr. J., 3 (1963), pp. 245–255.

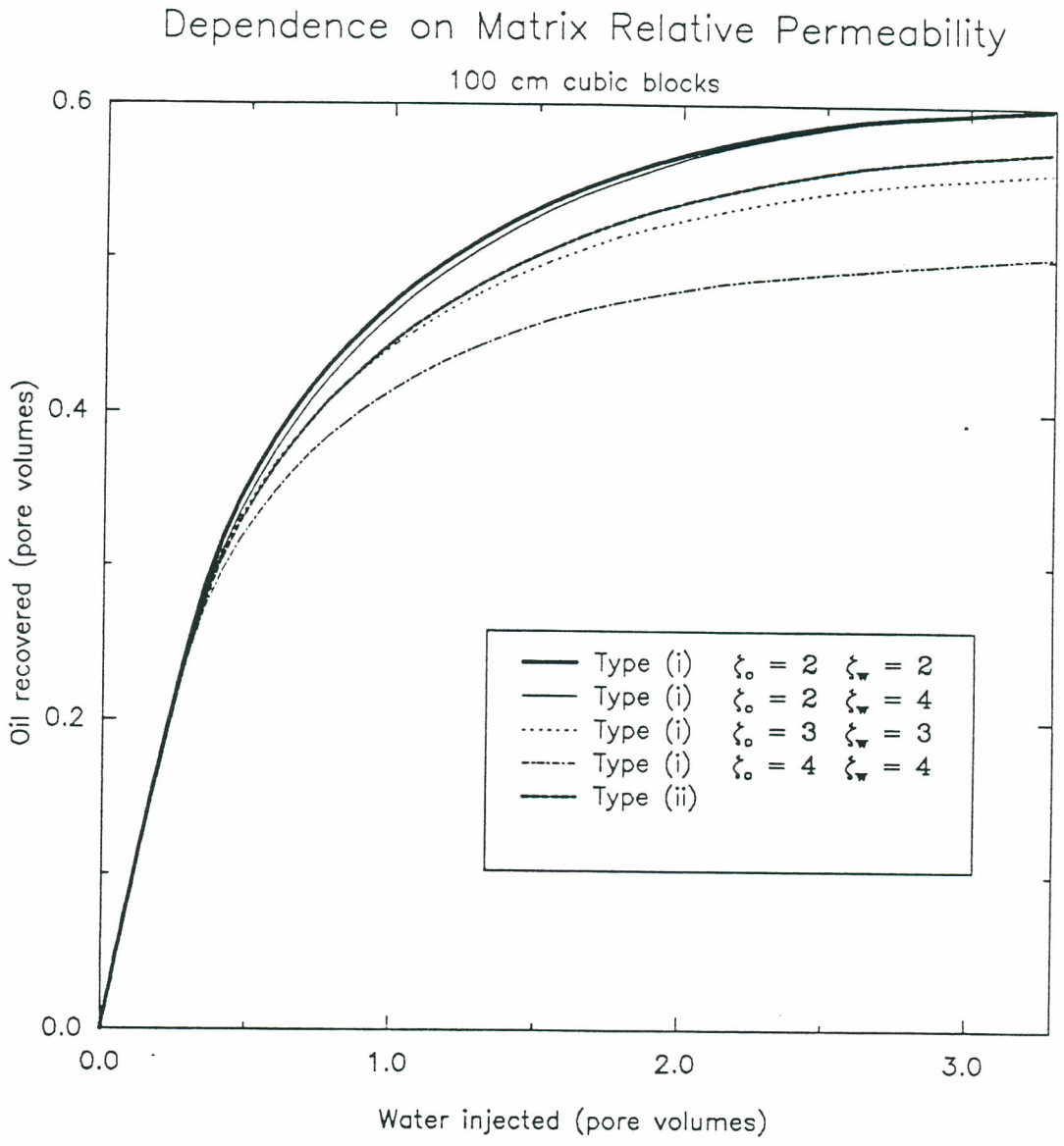
Dependence on Matrix Relative Permeability
100 cm cubic blocks
0.6
0.4
0.2
0.0
Oil recovered (pore volumes)
0.0
1.0
2.0
3.0
Water injected (pore volumes)
Type (i) $\zeta_o = 2$ $\zeta_w = 2$
Type (i) $\zeta_o = 2$ $\zeta_w = 4$
Type (i) $\zeta_o = 3$ $\zeta_w = 3$
Type (i) $\zeta_o = 4$ $\zeta_w = 4$
Type (ii)

**Figure 1**

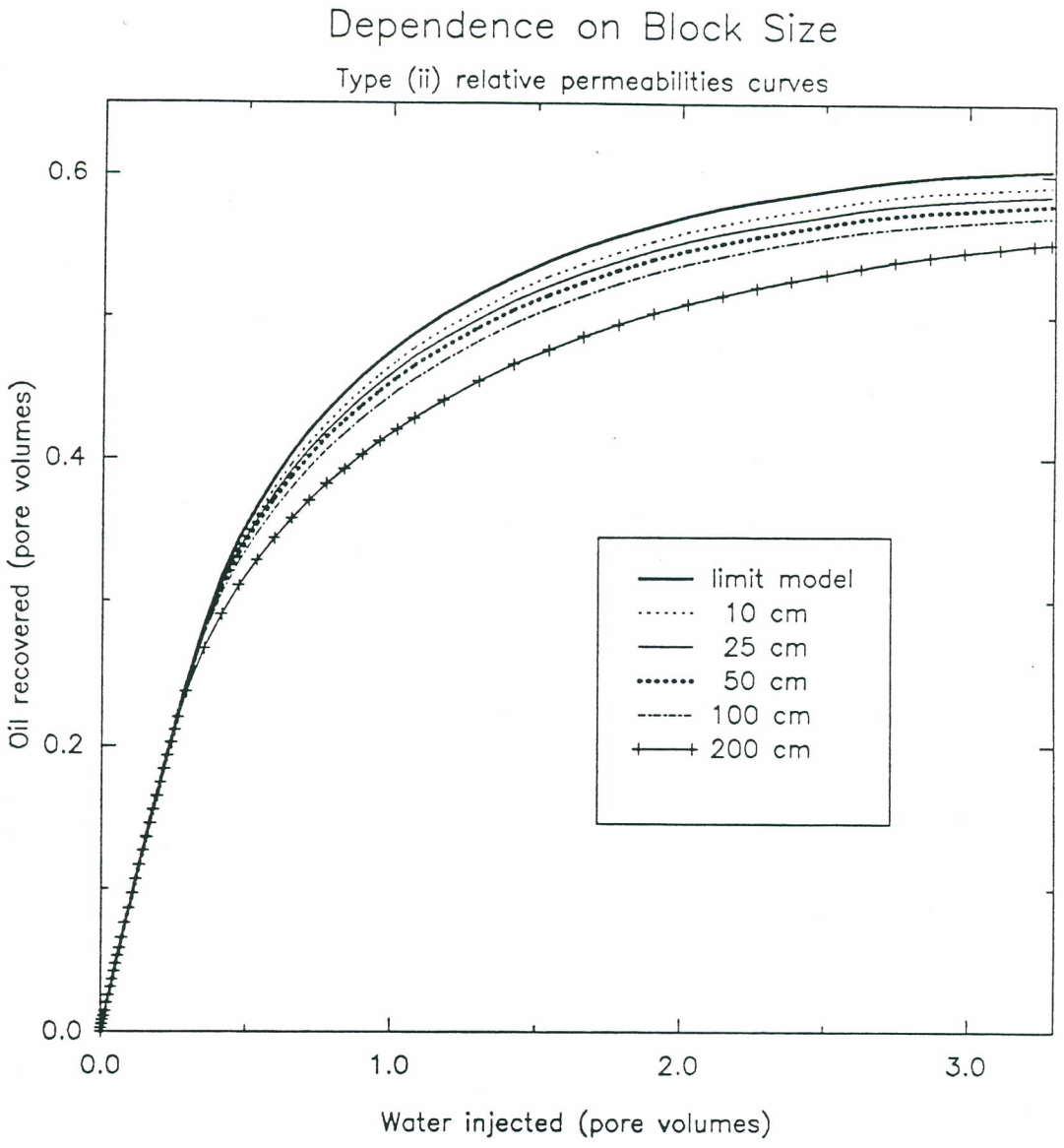
Dependence on Block Size
Type (ii) relative permeabilities curves
Oil recovered (pore volumes)
0.0
0.2
0.4
0.6
0.0
1.0
2.0
3.0
Water injected (pore volumes)
limit model
10 cm
25 cm
50 cm
100 cm
200 cm

**Figure 2**

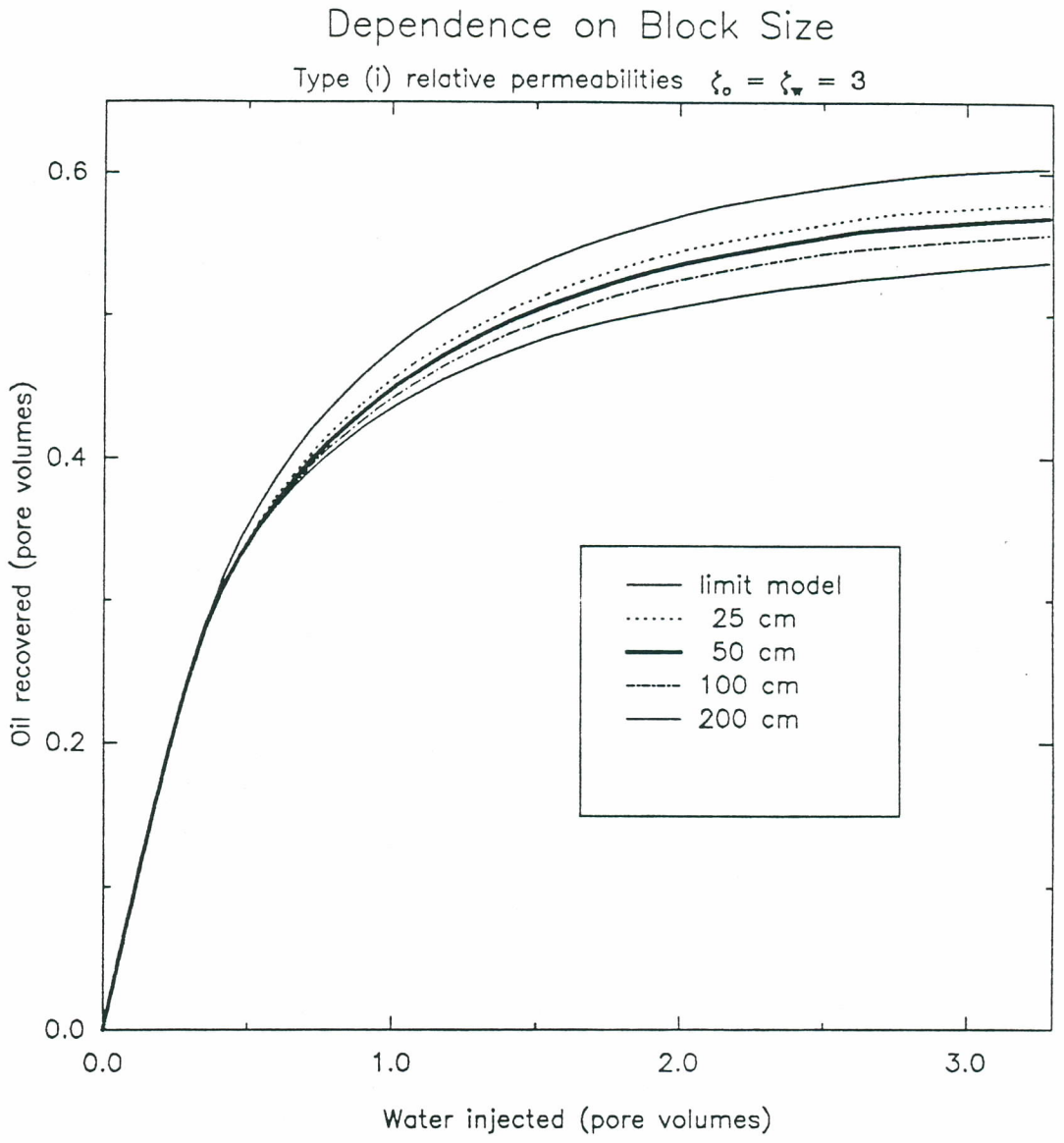
Dependence on Block Size
Type (i) relative permeabilities $\zeta_o = \zeta_w = 3$
0.6
0.4
0.2
0.0
Oil recovered (pore volumes)
0.0
1.0
2.0
3.0
Water injected (pore volumes)
limit model
25 cm
50 cm
100 cm
200 cm

**Figure 3**

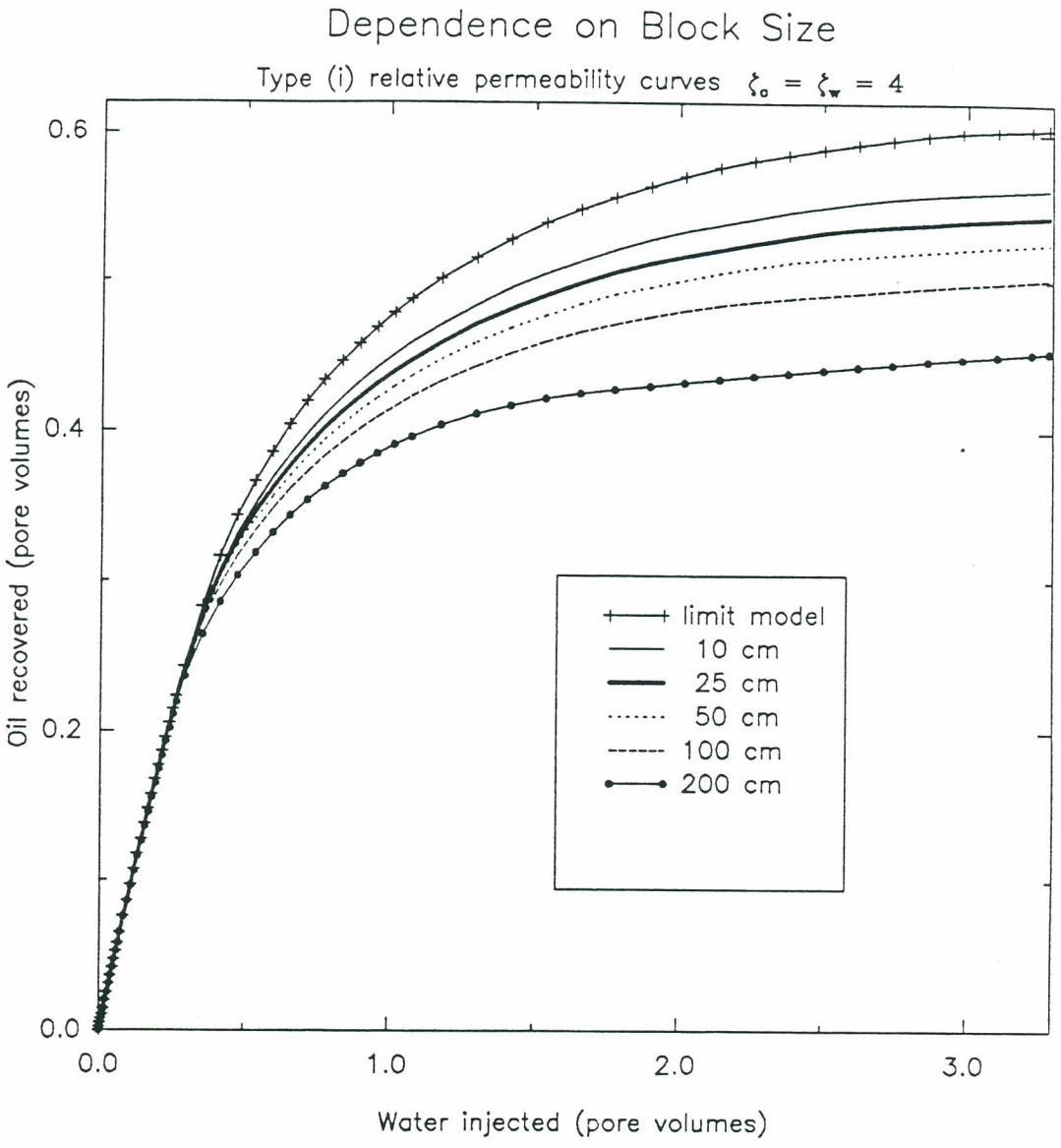
Dependence on Block Size
Type (i) relative permeability curves $\zeta_o = \zeta_w = 4$
Oil recovered (pore volumes)
0.0
0.2
0.4
0.6
0.0
1.0
2.0
3.0
Water injected (pore volumes)
limit model
10 cm
25 cm
50 cm
100 cm
200 cm

**Figure 4**

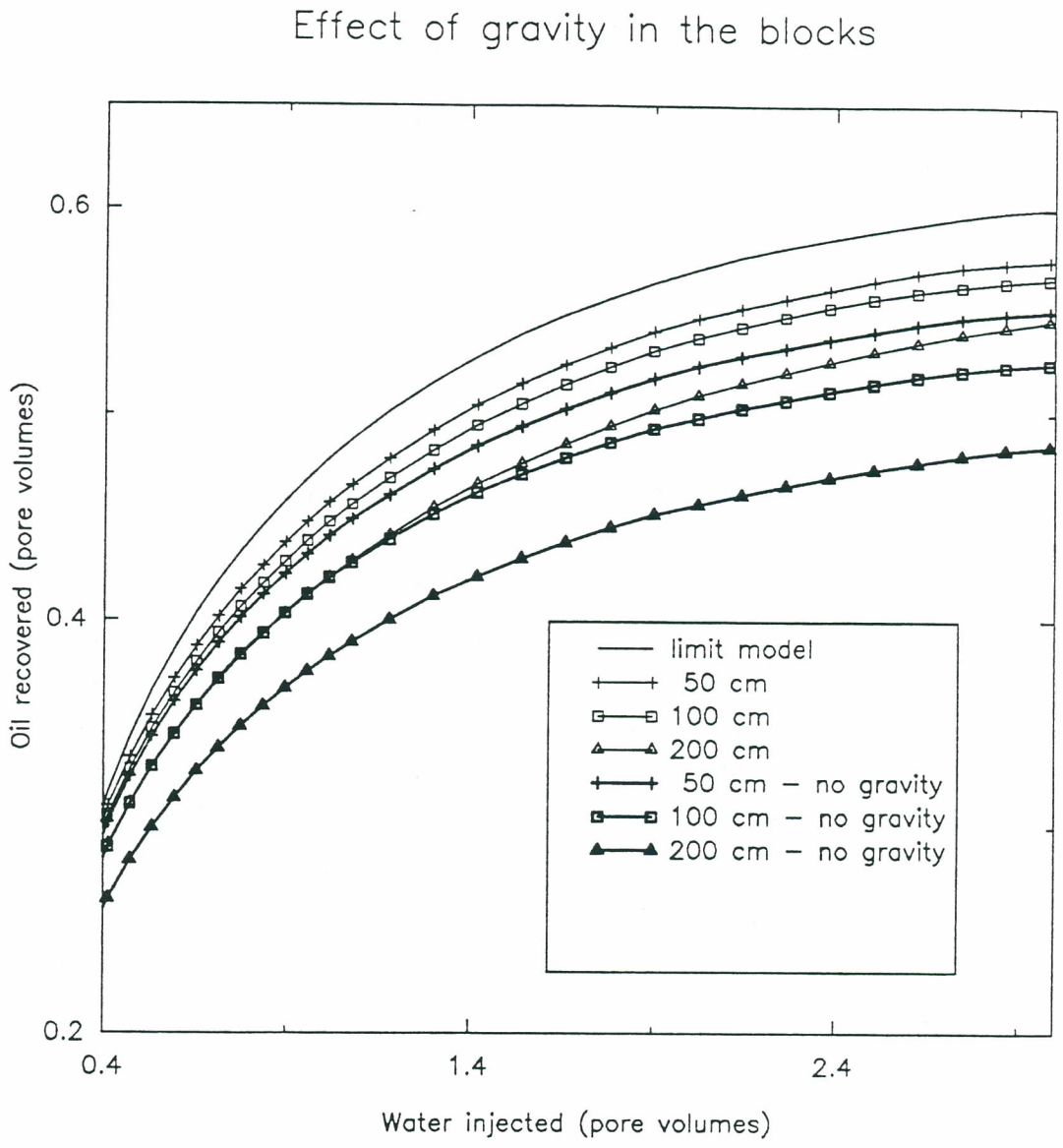
Effect of gravity in the blocks
0.6
0.4
0.2
Oil recovered (pore volumes)
0.4
1.4
2.4
Water injected (pore volumes)
limit model
50 cm
100 cm
200 cm
50 cm – no gravity
100 cm – no gravity
200 cm – no gravity

**Figure 5**

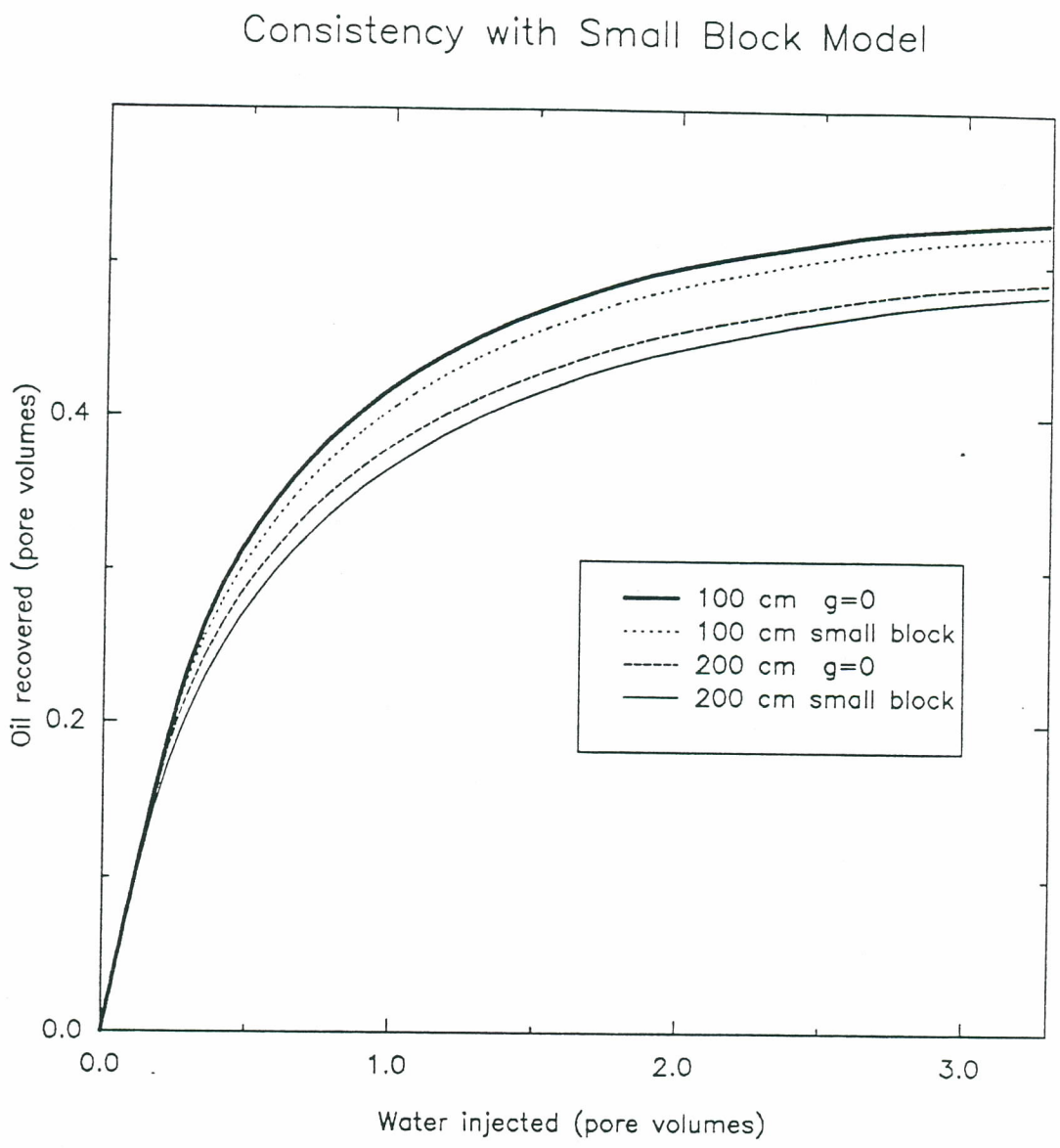
Consistency with Small Block Model
Oil recovered (pore volumes)
0.0
0.2
0.4
0.0
1.0
2.0
3.0
Water injected (pore volumes)
100 cm g=0
100 cm small block
200 cm g=0
200 cm small block

**Figure 6**

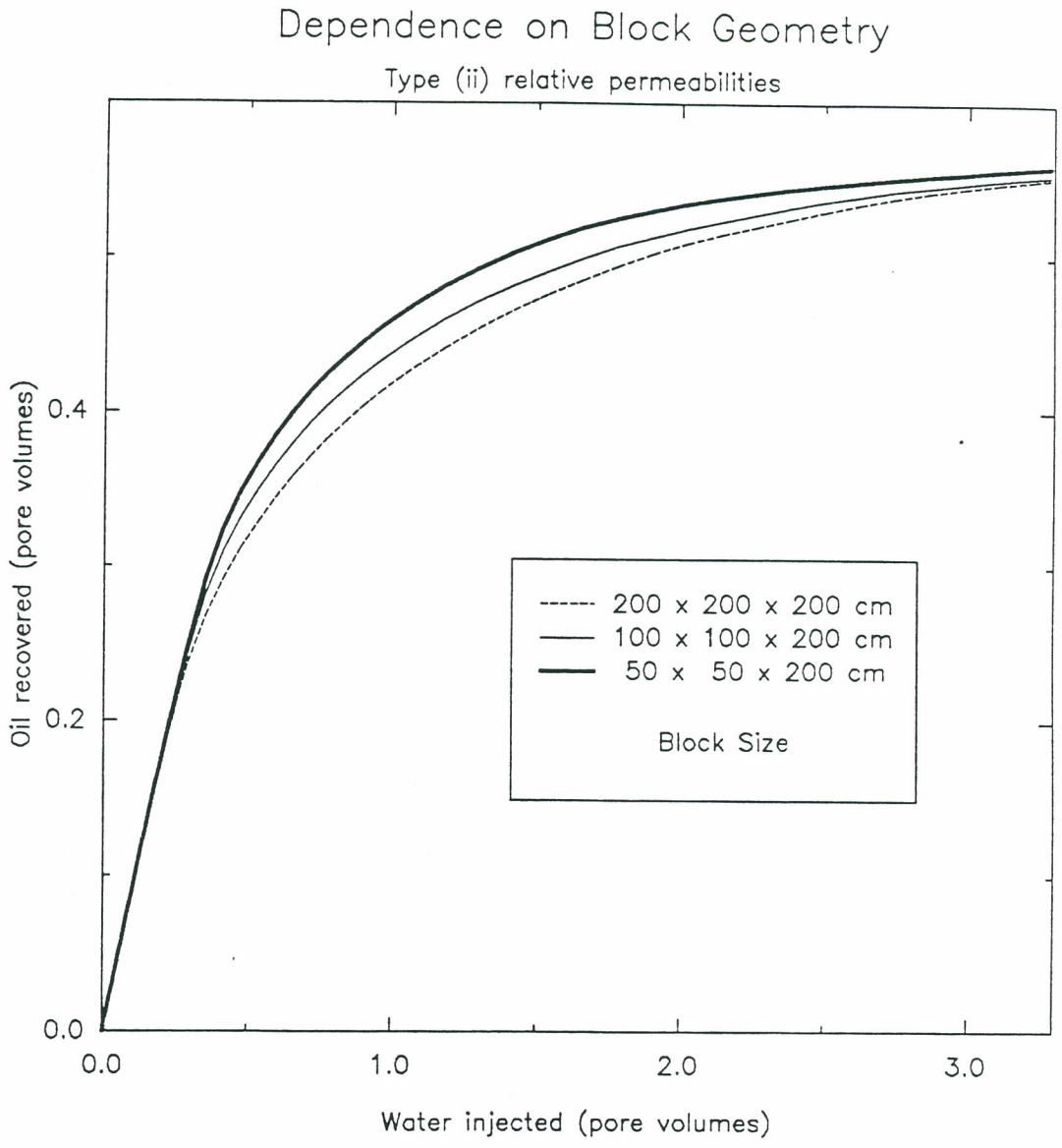
Dependence on Block Geometry
Type (ii) relative permeabilities
Oil recovered (pore volumes)
0.0
0.2
0.4
0.0
1.0
2.0
3.0
Water injected (pore volumes)
200 x 200 x 200 cm
100 x 100 x 200 cm
50 x 50 x 200 cm
Block Size

**Figure 7**

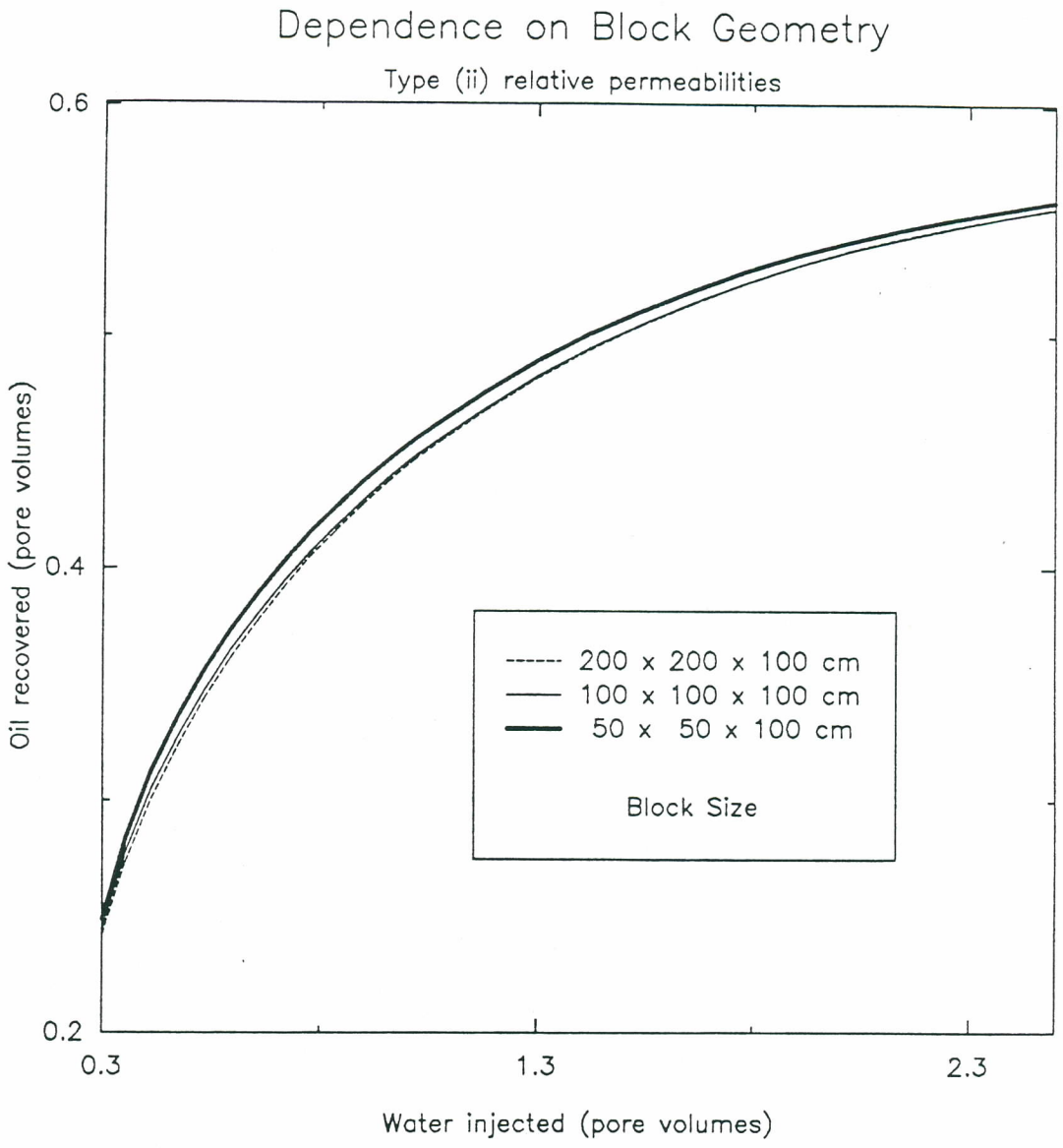
Dependence on Block Geometry
Type (ii) relative permeabilities
0.6
0.4
0.2
Oil recovered (pore volumes)
0.3
1.3
2.3
Water injected (pore volumes)
200 x 200 x 100 cm
100 x 100 x 100 cm
50 x 50 x 100 cm
Block Size

**Figure 8**

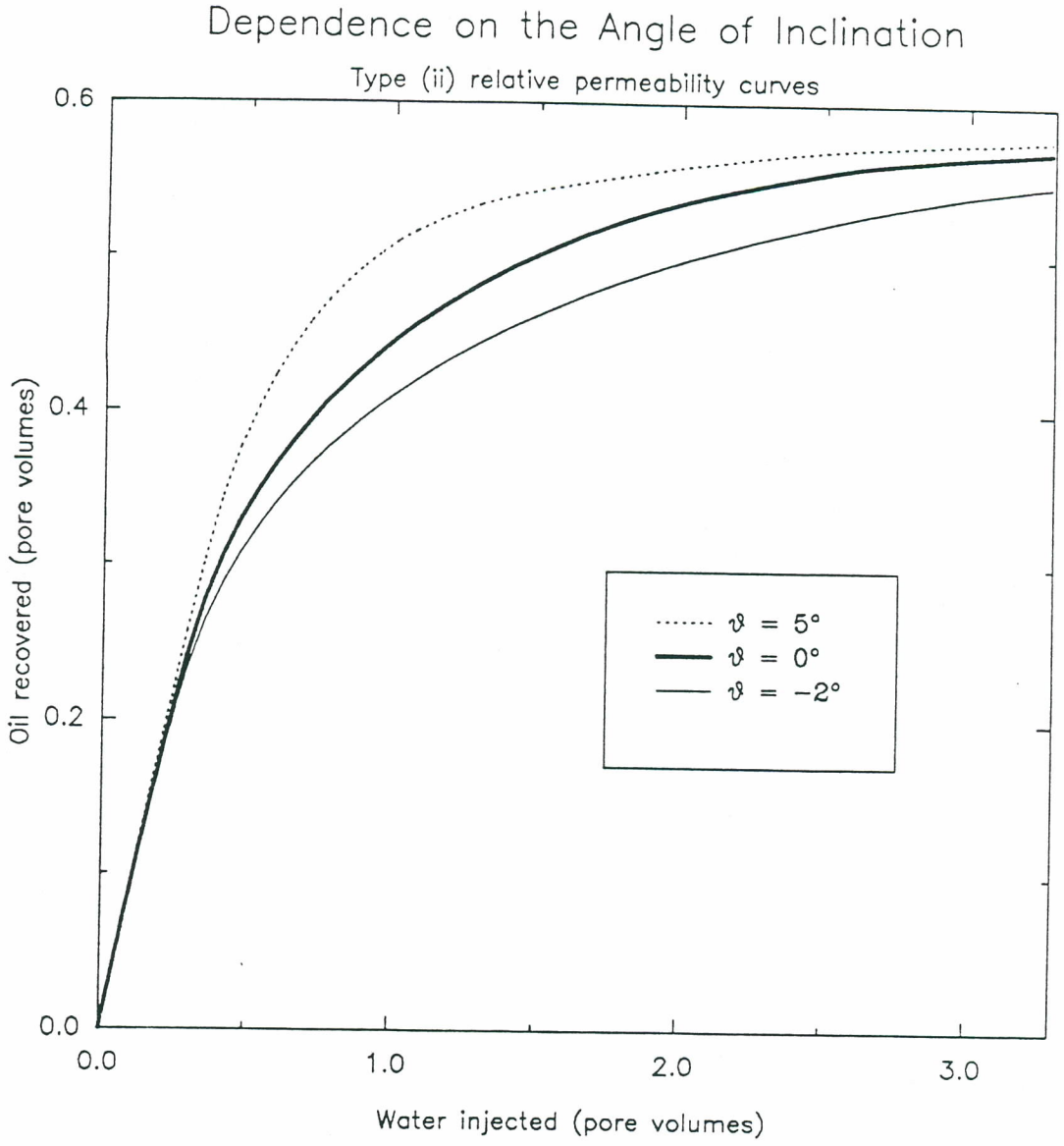
Dependence on the Angle of Inclination
Type (ii) relative permeability curves
0.6
0.4
0.2
0.0
Oil recovered (pore volumes)
0.0
1.0
2.0
3.0
Water injected (pore volumes)
ϑ = 5°
ϑ = 0°
ϑ = −2°

**Figure 9**

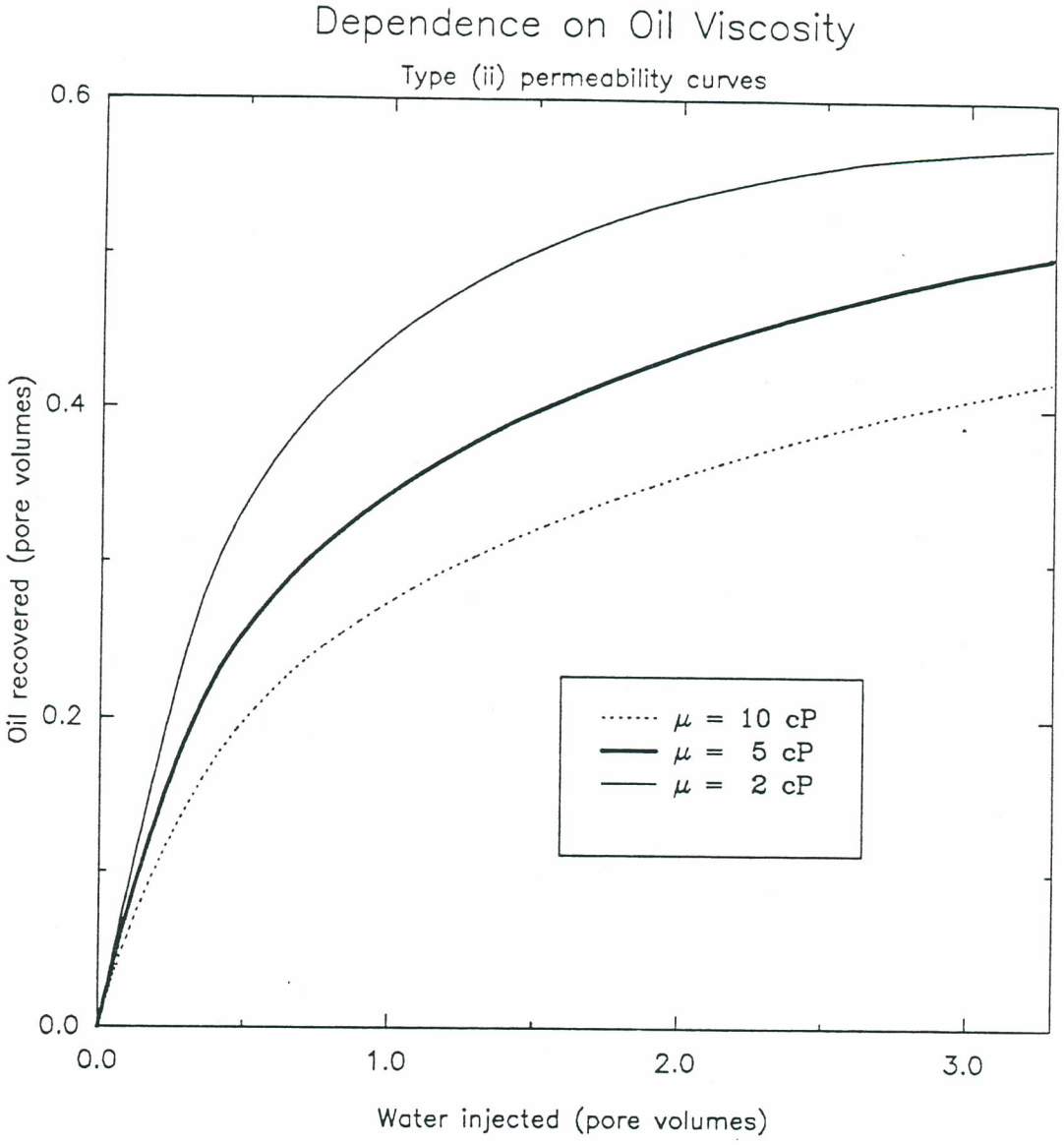
Dependence on Oil Viscosity
Type (ii) permeability curves
0.6
0.4
0.2
0.0
Oil recovered (pore volumes)
0.0
1.0
2.0
3.0
Water injected (pore volumes)
μ = 10 cP
μ = 5 cP
μ = 2 cP

**Figure 10**

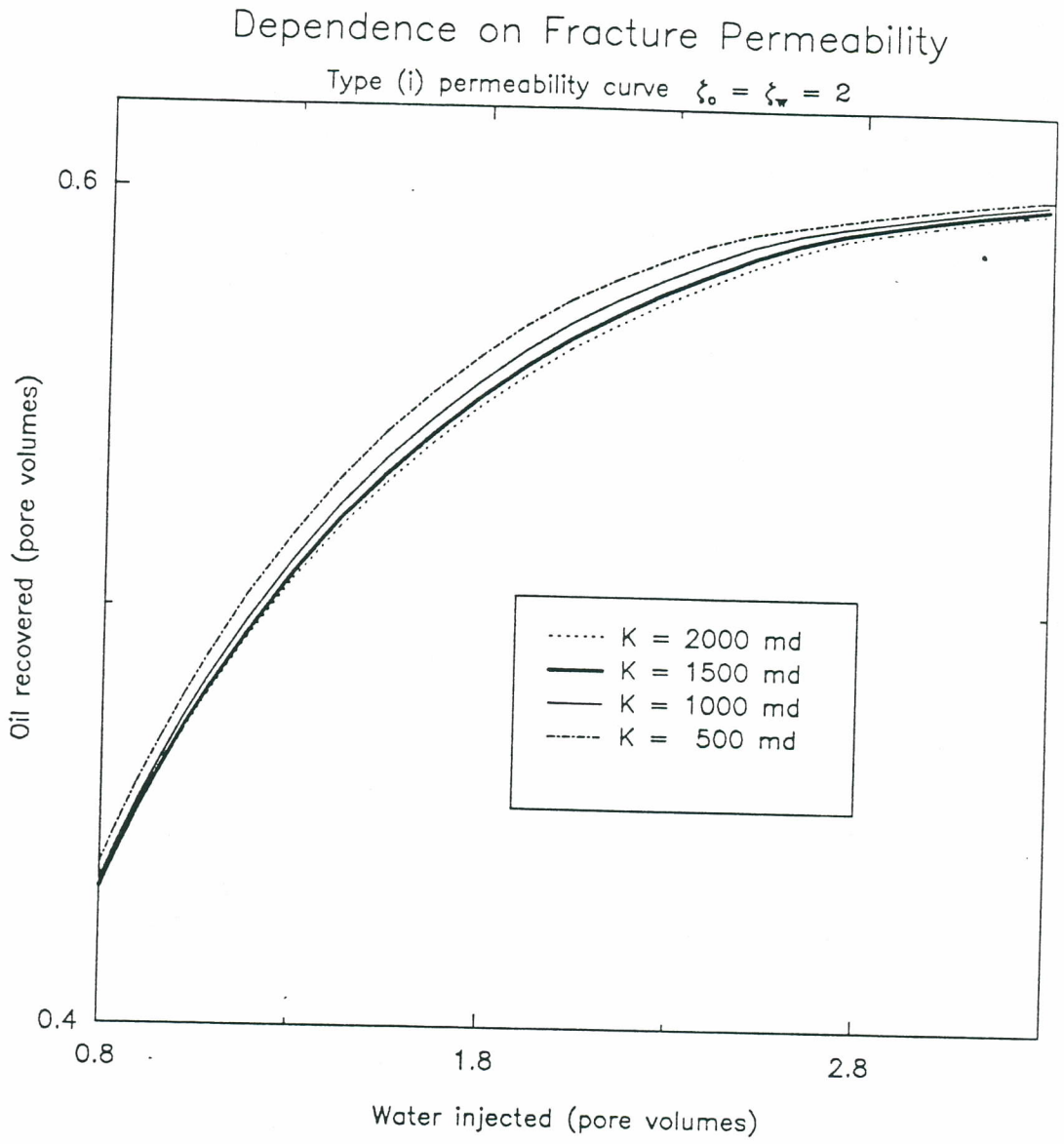
Dependence on Fracture Permeability
Type (i) permeability curve $\zeta_o = \zeta_w = 2$
0.6
0.4
0.8
1.8
2.8
Oil recovered (pore volumes)
Water injected (pore volumes)
K = 2000 md
K = 1500 md
K = 1000 md
K = 500 md

**Figure 11**